Chapter 3
Hadron Structure on the Lattice

K.U. Can, A. Kusno, E.V. Mastropas, and J.M. Zanotti

Abstract The aim of these lectures will be to provide an introduction to some of the concepts needed to study the structure of hadrons on the lattice. Topics covered include the electromagnetic form factors of the nucleon and pion, the nucleon's axial charge and moments of parton and generalised parton distribution functions. These are placed in a phenomenological context by describing how they can lead to insights into the distribution of charge, spin and momentum amongst a hadron's partonic constituents. We discuss the techniques required for extracting the relevant matrix elements from lattice simulations and draw attention to potential sources of systematic error. Examples of recent lattice results are presented and are compared with results from both experiment and theoretical models.

3.1 Introduction

The proton was believed to be a point-like particle until the measurement of its magnetic moment by Nobel-Prize laureate Otto Stern in 1933. The significant deviation of the measured value $\mu_p \approx 2.5\mu_N$ from the unit nuclear magneton $\mu_N = e/2M_N$, where M_N is the nucleon mass, provided first evidence for the composite nature of the proton. The latest CODATA value now indicates that $\mu_p = 2.792847356(23)\mu_N$. Our modern understanding is that the nucleon is not a point-like particle but a colour-singlet bound state of the fundamental building blocks of hadronic matter: quarks and gluons. It is a challenge, however, to understand

K.U. Can (✉)
Department of Physics, H-27, Tokyo Institute of Technology, Meguro, Tokyo 152-8551 Japan
e-mail: utku.can@th.phys.titech.ac.jp

A. Kusno • E.V. Mastropas
Department of Physics, College of William and Mary, P.O. Box 8795, Williamsburg VA 23187-8795, USA
e-mail: akusno@email.wm.edu; emastropas@email.wm.edu

J.M. Zanotti
CSSM, School of Chemistry and Physics, The University of Adelaide, Adelaide SA 5005, Australia
e-mail: james.zanotti@adelaide.edu.au

H.-W. Lin, H.B. Meyer (eds.), *Lattice QCD for Nuclear Physics*, Lecture Notes in Physics 889, DOI 10.1007/978-3-319-08022-2_3

how these constituents are distributed inside the nucleon and how they combine to give the nucleon its fundamental properties. We can immediately think of questions like: being a charge neutral object, does the neutron have a charged core in analogy with an atom or is the charge distributed homogeneously? How do the constituents combine to form the different hadrons? And can we find unravel the spin structure of the proton?

The electromagnetic current is the perfect probe for investigating the charge and magnetisation distributions of the nucleon, whereas the axial-vector current can resolve the spin structure. For instance, it is still a mystery as to how much of the spin of the proton is carried by quarks and gluons. Deep-inelastic scattering experiments, for example, indicate that only $1/3$ of the proton's spin is carried by quarks and antiquarks [131,132]. This problem was originally known as the "proton-spin crisis" and demonstrates that questions still remain as to the fundamental structure of hadrons.

Experimental probes of nucleon electromagnetic structure are based on electron-proton scattering processes, since QED is a well-understood theory, and its small fine-structure constant allows perturbative calculations. From the experimental point of view it is also easy to accelerate electrons and tune their energies to desired values. The electron-proton scattering processes can be considered in two categories: elastic and deep-inelastic scattering.

In these lecture notes, we will first introduce some of the phenomenological quantities used to assist in our understanding of nucleon structure and some of the experimental processes used to determine them. We then turn our attention to studying some of the techniques used to study these same quantities on the lattice, together with some detailed examples for the more common calculations. We will finish by placing the lattice methods in context by highlighting a couple of recent results and comparing them to experimental determinations.

3.2 Experimental Probes

3.2.1 Elastic $e-p$ Scattering

In elastic electron-nucleon scattering, the electron interacts with the nucleon via photons and leaves the nucleon intact but with recoil. This process is dominated by single-photon exchange, and it is possible to map out the charge and magnetisation-density distributions of the nucleon by varying the momentum transferred to the nucleon target. If we consider the nucleon to be a point-like particle, we can describe the interaction cross section of this process with the Mott formula:

$$\left(\frac{d\sigma}{d\Omega}\right)_{\text{point}} = \frac{(Z\alpha)^2 E^2}{4k^2 \sin^4(\theta/2)} \left(1 - \frac{k^2}{E^2} \sin^2(\theta/2)\right), \tag{3.1}$$

where Z is the atomic (proton) number, α is the fine-structure constant, E and k are the energy and momentum of the incoming electron, and θ is the scattering angle described as $q^2 = -4EE' \sin^2(\theta/2)$, with E' the outgoing electron energy and q the transfer momentum. However, experimental data shows a clear deviation from the point-like cross section, indicating that the nucleon has some internal structure. So it is necessary to reconsider the cross-section formula and include a term that depends on q^2,

$$\frac{d\sigma}{d\Omega} = \left(\frac{d\sigma}{d\Omega}\right)_{\text{point}} \left|F(q^2)\right|^2 . \tag{3.2}$$

3.2.1.1 Rosenbluth Formula

We will attempt to rewrite the cross section starting from the S-matrix. For simplicity, we will consider only the tree-level diagram, however, since the fine-structure constant is small and one-photon exchange diagrams dominate the process. This was expected to be a safe approximation, but in fact it is now known that the inclusion of two-photon exchange effects are vital (see, e.g., [133]), especially at large q^2; nonetheless, we will not consider these here. The S-matrix is given by

$$\begin{aligned} S &= (2\pi)^4 \delta^4(k + P - P' - k')\bar{u}(k')(-ie\gamma^\mu)u(k)\frac{-i}{q^2}\left\langle P'|(ie)J_\mu|P\right\rangle \\ &= -i(2\pi)^4 \delta^4(k + P - P' - k')\mathcal{M}\,, \end{aligned} \tag{3.3}$$

where the Dirac-delta function ensures energy-momentum conservation, $\bar{u}(k')$ and $u(k)$ are the fermion spinor fields with four-momenta k and k', $(-ie\gamma^\mu)$ is the electron-photon vertex, and $\langle P'|(ie)J_\mu|P\rangle$ the photon-nucleon vertex. In the second step we have introduced the invariant amplitude $\mathcal{M}$,

$$\mathcal{M} = \frac{1}{q^2}\bar{u}(k')(-ie\gamma^\mu)u(k)\langle P'|(ie)J_\mu|P\rangle. \tag{3.4}$$

The electromagnetic current is

$$J^\mu = \sum_i e_i \bar{\psi}_i \gamma^\mu \psi_i\,, \tag{3.5}$$

where the index i sums over all quark flavours with $m_q \ll m_p$, namely the up, down and strange quarks. The cross section in terms of invariant amplitude can be written as

$$d\sigma = \frac{E'}{2EM^2}\frac{1}{1 + \frac{2E}{M}\sin^2(\theta/2)}|\mathcal{M}|^2\frac{d\Omega}{(2\pi)^2}\,, \tag{3.6}$$

where E' is the energy of the scattered electron, and we write the squared invariant amplitude in terms of leptonic and hadronic tensors:

$$|\mathcal{M}|^2 = \frac{e^4}{Q^4} \ell^{\mu\nu} W_{\mu\nu} \,. \tag{3.7}$$

Here $-q^2 = Q^2$, the leptonic tensor is defined as

$$\ell^{\mu\nu} = \bar{u}(k')\gamma^\mu u(k)\bar{u}(k)\gamma^\nu u(k'), \tag{3.8}$$

and the hadronic tensor as

$$W^{\mu\nu} = \left\langle P|J^\nu|P'\right\rangle \langle P'|J^\mu|P\rangle \,. \tag{3.9}$$

The above hadronic matrix element between nucleon states is defined by two Lorentz-invariant form factors (FFs),

$$\langle P'|J^\mu(\boldsymbol{q})|P\rangle = \bar{u}(P')\left[\gamma^\mu F_1(q^2) + i\sigma^{\mu\nu}\frac{q_\nu}{2M}F_2(q^2)\right]u(P), \tag{3.10}$$

with $\sigma^{\mu\nu} = \frac{i}{2}[\gamma^\mu, \gamma^\nu]$ and M being the mass of the nucleon. F_1 and F_2 are referred to as the Dirac and Pauli form factors, respectively. Using the fact that both tensors are symmetric and conserved (i.e. $q^\mu \ell_{\mu\nu} = q^\mu W_{\mu\nu} = 0$), the elastic scattering cross-section in the lab frame can be written as

$$\frac{d\sigma}{d\Omega} = \sigma_{\text{Mott}}\left[\frac{G_E^2(Q^2) + \tau G_M^2(Q^2)}{1+\tau} + 2\tau G_M^2(Q^2)\tan^2\frac{\theta}{2}\right], \tag{3.11}$$

where we have defined the Sachs electric and magnetic FFs,

$$\begin{aligned} G_E(Q^2) &= F_1(Q^2) - \tau F_2(Q^2), \\ G_M(Q^2) &= F_1(Q^2) + F_2(Q^2), \end{aligned} \tag{3.12}$$

in terms of F_1 and F_2 and the factor $\tau = Q^2/4M^2$. Rewriting the cross section in terms of the virtual photon's longitudinal polarisation $\epsilon = (1 + (1 + \tau)2\tan^2(\theta/2))^{-1}$, we end up with the Rosenbluth formula,

$$\frac{d\sigma}{d\Omega} = \frac{\sigma_{\text{Mott}}}{1+\tau}\left[G_E^2(Q^2) + \frac{\tau}{\epsilon}G_M^2(Q^2)\right] \,. \tag{3.13}$$

So we see that it is possible to extract the electric and magnetic form factors from the slope and intercept of a curve fitted to the experimental cross section plotted as a function of scattering angle at fixed momentum transfer Q^2. This is known as the Rosenbluth separation technique. We note from Eq. (3.13), however, that the

coefficient of G_E is suppressed at large Q^2, and hence the cross section is dominated by G_M in this domain. Therefore, it is harder to extract information on G_E^2 at large momentum transfers.

3.2.1.2 Polarisation Transfer

Given the shortcomings of the Rosenbluth separation technique in extracting accurate results for the electric form factor at large Q^2, it is clear that there is a need for new experimental methods. The need for polarisation-transfer techniques was pointed out in several papers [134–137]. With advances in experimental techniques such as highly polarised and high-luminosity electron beams, polarised targets (e.g ^{1}H, ^{2}H, ^{3}He) and large and efficient neutron detectors, the polarisation-transfer experiments began to give us more insight about the nucleon's structure.

It is possible to obtain the ratio G_E^p/G_M^p from the elastic scattering of longitudinally polarised electrons from unpolarised protons in terms of the transferred polarisation components perpendicular (P_t) and parallel (P_l) to the recoil proton's momentum in the scattering plane [135, 137],

$$\frac{G_E^p}{G_M^p} = -\frac{P_t}{P_l}\frac{E+E'}{2M}\tan\left(\frac{\theta}{2}\right), \tag{3.14}$$

where E and E' are the incident and scattered electron energy, respectively, and θ is the electron scattering angle.

A recent analysis by the JLab Hall-A Collaboration [138] showed that, unlike the conventional Rosenbluth-method estimation which provided $\mu_p G_E^p/G_M^p \approx 1$, the proton form-factor ratio clearly deviates from unity. Figure 3.1 from [138] shows the behaviour of this ratio.

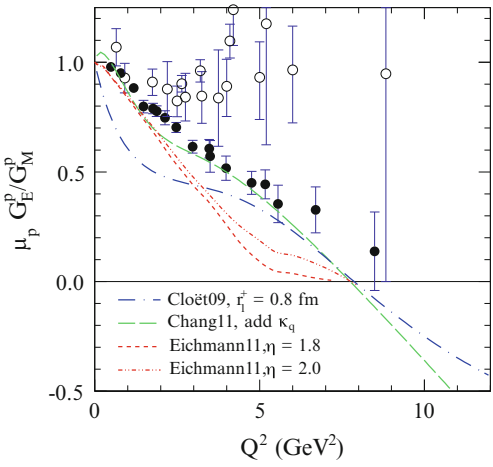

Fig. 3.1 Experimental data with fitted predictions based on Dyson-Schwinger equation calculations. *Empty circles* indicate the unpolarised, whereas the *filled ones* are obtained from polarisation-transfer experiments. Figure from [138]

It is evident that the G_E^p falls faster than G_M^p, and their Q^2 dependences differ. If the planned experiments forming part of the JLab upgrade[1] find the slope of the linear fall stays unchanged, then it might lead to the conclusion that G_E^p changes sign. One last note is that the discrepancy between the Rosenbluth and polarisation-transfer methods is believed to be due to the two-photon exchange (TPE) radiative corrections to the cross-section measurements. A broad discussion about TPE can be found in [133] and references therein.

3.2.1.3 Physical Interpretation

The physical interpretation of the electric and magnetic form factors is that for small Q^2, or in the limit $M \to \infty$ such that $Q^2 \ll M^2$, we can assume that the initial- and final-state nucleons are fixed at the same location and that they have the same internal structure. We then have the physical interpretation that the Fourier transforms of the form factors lead to density distributions. However, since M is finite, one should consider nucleon recoil effects with increasing Q^2. In this case, the initial and final nucleon states no longer have the same momentum, thus their wavefunctions differ (i.e. there is a relative Lorentz contraction), and it is no longer possible to have a probability or density interpretation [139].

One method for circumventing this issue is to consider the Breit frame where the initial and final momenta of the nucleon have the same magnitude. In this case, the initial- and final-state nucleon wavefunctions are sampled in the same frame, and we recover our density-distribution interpretation.

An alternative frame that also retains the density-distribution interpretation of form factors in a model-independent way is given by the infinite-momentum frame where the parton (quark) charge density in transverse space is given as a two-dimensional Fourier transformation of F_1,

$$\rho(b) = \int \frac{d^2\mathbf{q}_\perp}{(2\pi)^2} e^{-i\mathbf{b}_\perp \cdot \mathbf{q}_\perp} F_1(Q^2 = \mathbf{q}_\perp^2), \tag{3.15}$$

where $\mathbf{q}_\perp$ and $\mathbf{b}_\perp$ are the momentum transfer and distance of the quark to the center of momentum, respectively, of a fast-moving nucleon in the longitudinal direction.

Pursuing the spatial density interpretation, we can expand the Fourier transform of such a distribution, which allows us to write the electric form factor as

$$G_E(Q^2) = \int d^3\mathbf{x}\, e^{i\mathbf{x}\cdot\mathbf{q}} \rho(\mathbf{x}) \simeq 1 - \frac{1}{6} Q^2 \langle r^2 \rangle + \ldots \tag{3.16}$$

[1] See for instance, http://www.jlab.org/exp_prog/12GEV_EXP/.

The charge radius of the nucleon is then defined by

$$\langle r^2 \rangle = -6 \left. \frac{dG_E(Q^2)}{dQ^2} \right|_{Q^2=0} . \tag{3.17}$$

We note here that there has been a lot of recent activity surrounding $r = \sqrt{\langle r_E^2 \rangle}$. Electron-proton scattering experiments found that the rms charge radius of the proton is $r = 0.875(8)(6)$ fm, in good agreement with the atomic-hydrogen Lamb-shift experiments and QED calculations [140]. Recent muonic-hydrogen Lamb-shift measurements, however, indicate $r = 0.84184(67)$ fm, showing a 5σ difference [141], which has yet to be resolved.

3.2.2 Deep-Inelastic Scattering

In the previous section, we saw how elastic electron-proton scattering can provide a framework in which to determine the electromagnetic form factors of the proton. While elastic scattering occurs at small enough energies so that the final proton would stay intact, we now consider an experimental process that occurs with high enough energy that the proton is "smashed" into many fragments. This is known as deep-inelastic scattering (DIS). The DIS process is dominated by a single quark in the nucleon which is "knocked out" by a virtual photon (see Fig. 3.2).

As in case of elastic scattering, let us start with the expression for the S-matrix for deep-inelastic scattering:

$$S = (2\pi)^4 \delta^4(k + P - P' - k') \bar{u}(k')(-ie\gamma^\mu) u(k) \frac{-i}{q^2} \langle X | (ie) J^\mu | P \rangle . \tag{3.18}$$

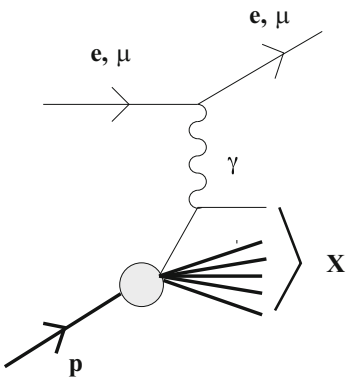

Fig. 3.2 Deep-inelastic scattering

We have here conservation of momentum $\delta^4(k + P - P' - k')$, a leptonic piece $\bar{u}(k')(-ie\gamma^\mu)u(k)$ which can be calculated in perturbation theory, and a hadronic piece $\langle X|(ie)J^\mu|P\rangle$. After smashing the initial proton with the probe, it is going to break up into many fragments, and for an inclusive process we need to include in the hadronic piece all possible final states, which we label X. The inclusive cross section can be written in the following form:

$$\frac{d\sigma}{d\Omega dE} = \frac{\alpha^2}{Q^4}\frac{E'}{E}\ell_{\mu\nu}W^{\mu\nu}. \tag{3.19}$$

Here $\ell_{\mu\nu}$ is the leptonic tensor, $W^{\mu\nu}$ is the hadronic tensor which itself is a square of the matrix element from Eq. (3.18), and we have here a sum over all possible final states

$$W_{\mu\nu} = \frac{1}{4\pi}\sum_X \langle P|J_\mu|X\rangle\langle X|J_\nu|P\rangle(2\pi)^4\delta^4(P + q - P_X). \tag{3.20}$$

Since the final states are summed over, the hadronic tensor $W^{\mu\nu}$ only depends on the initial proton momentum P and photon momentum q. Using Lorentz symmetry, parity and time-reversal invariance and current conservation, we can express this hadronic tensor in terms of two invariant tensors

$$\begin{aligned} W_{\mu\nu} = {} & W_1\left(-g^{\mu\nu} + \frac{q^\mu q^\nu}{q^2}\right) \\ & + \frac{W_2}{M^2}\left(P^\mu - q^\mu\frac{(P\cdot q)}{q^2}\right)\left(P^\nu - q^\nu\frac{(P\cdot q)}{q^2}\right), \end{aligned} \tag{3.21}$$

where W_1 and W_2 are the so-called structure functions of the proton which depend on two variables: the 4-momentum transfer squared

$$Q^2 = -q^2, \tag{3.22}$$

and the energy transferred to the nucleon by the scattering electron

$$\nu = \frac{P\cdot q}{M}. \tag{3.23}$$

The early data from SLAC indicated that these structure functions W_1 and W_2 are nearly independent of Q^2 when plotted as a function of the dimensionless combination

$$x = -\frac{q^2}{2P\cdot q} = \frac{Q^2}{2M\nu}. \tag{3.24}$$

This effect is known as Bjorken scaling, and x is called the Bjorken scaling variable, although as we will discuss later, small scaling violations are observed at small x.

3.2.2.1 Parton Model

If we work at fixed x, the limit of $Q^2 \to \infty$ is known as the Bjorken limit. The effect of Bjorken scaling in this limit led Feynman to introduce the "parton model". According to his idea, the inelastic electron-proton scattering is a sum of elastic scatterings of the electron on free partons within the proton (the term parton refers to any particle with no internal structure). A key factor for investigating the proton substructure is the wavelength of the probe

$$\lambda \sim \frac{1}{\sqrt{Q^2}}, \tag{3.25}$$

and, of course, at large momentum transfer we are going to have higher resolution; Fig. 3.3 represents it diagrammatically. If Q^2 is small (i.e. the wavelength is large), then the probe will only resolve the proton as a whole, but if we increase the value of Q^2 (decrease the wavelength of the probe), this means that we will be able to resolve quantities inside of the hadron, so the probe will "see" quarks rather than a proton. This picture is also valid for a fast-moving nucleon, i.e. the infinite-momentum frame.

In the Bjorken limit, one defines the functions

$$F_1(x) = \lim_{Q^2 \to \infty} W_1(Q^2, \nu), \tag{3.26}$$

$$F_2(x) = \lim_{Q^2 \to \infty} \frac{\nu}{M} W_2(Q^2, \nu). \tag{3.27}$$

And in Feynman's parton model, the structure functions are sums of the parton densities f_i constituting the proton:

$$F_1(x) = \frac{1}{2} \sum_i e_i^2 f_i(x), \tag{3.28}$$

$$F_2(x) = x \sum_i e_i^2 f_i(x)\,, \tag{3.29}$$

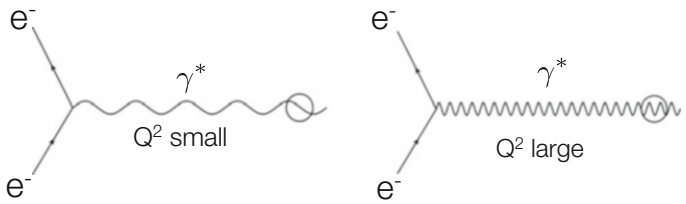

Fig. 3.3 Large momentum transfer leads to higher resolution. The left diagram represents resolving a proton at small Q^2, while the right diagram has a Q^2 high enough for investigating proton substructure (quarks)

where for quarks, the charge e_i is also included. f_i is the probability that the struck parton, i, carries a fraction, x, of the proton momentum, and is called a parton distribution function (PDF). Since the total probability must be 1, we have

$$\sum_i \int_0^1 dx\, x f_i(x) = 1. \tag{3.30}$$

Results from DIS tell us that the fraction of the nucleon momentum carried by the quarks $\int dx\, xq(x)$ is only about 50 % (here $q(x) = f_q(x)$). This gives us an idea that gluons must play a very important role in the structure of the nucleon by carrying roughly half of its momentum. In fact, much of our knowledge about QCD and the structure of the nucleon has been derived from DIS experiments. They told us that there are two up and one down valence quarks with electric charge $2/3$ and $-1/3$ in the proton; the number of quarks is infinite because the integral over parton densities $\int dx\, q(x)$ does not seem to converge, so there is an infinite number of quark-antiquark pairs living inside of the proton.

3.2.2.2 Parton Distribution Functions

Let us take a look at how these PDFs might look. For a point nucleon (i.e. if we consider the nucleon as a single parton with no internal structure which carries all momentum), F_2 is a delta function at $x = 1$ (Fig. 3.4). If the nucleon is made up of three quarks which equally share the momentum, then each quark carries $1/3$ of the momentum, and we will have a delta function at $1/3$, as in Fig. 3.5. If the three quarks are interacting, which means that they are exchanging some gluons, then they can share momentum. So the PDF is going to be smeared around the peak of $1/3$ (see Fig. 3.6). Finally, we should consider the case with sea quarks. Here, one quark emits a gluon which turns into quark-antiquark pair, and then all valence quarks in $q\bar{q}$ loop must have lower x than the original quark. Therefore, in Fig. 3.7 we should see an enhancement at small x.

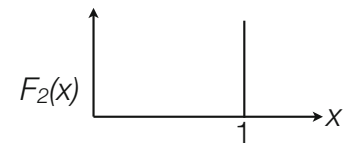

Fig. 3.4 PDF for a point nucleon

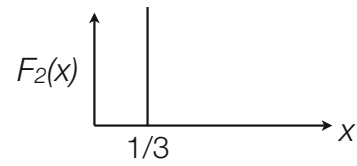

Fig. 3.5 PDF for a nucleon with three quarks

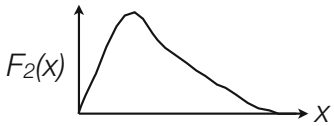

Fig. 3.6 PDF for three interacting quarks

Fig. 3.7 Enhancement at small x for the nucleon with sea quarks

The proton contains two up and one down quarks which are termed "valence" quarks: $u_v(x)$, $d_v(x)$. It is possible that a valence quark radiates a gluon which then turns into a quark-antiquark pair which are termed "sea" quarks, and we are going to call PDFs associated with $u_s(x)$, $d_s(x)$, $s_s(x)$. Then we can write the proton and neutron structure functions as following (ignoring heavy quarks):

$$F_2^p(x) = x\left\{\frac{4}{9}\left[u^p(x)+\bar{u}^p(x)\right]+\frac{1}{9}\left[d^p(x)+\bar{d}^p(x)\right]+\frac{1}{3}\left[s^p(x)+\bar{s}^p(x)\right]\right\}, \tag{3.31}$$

$$F_2^n(x) = x\left\{\frac{4}{9}\left[u^n(x)+\bar{u}^n(x)\right]+\frac{1}{9}\left[d^n(x)+\bar{d}^n(x)\right]+\frac{1}{3}\left[s^n(x)+\bar{s}^n(x)\right]\right\}, \tag{3.32}$$

where total PDF of any particular flavour in Eqs. (3.31), (3.32) is

$$q \equiv q_v + q_s. \tag{3.33}$$

Under isospin flip $u \leftrightarrow d$ and $p \leftrightarrow n$, assuming charge symmetry means that the distribution of the up quarks in the proton is the same as distribution of the down quarks in the neutron:

$$u(x) \equiv u^p(x) = d^n(x), \tag{3.34}$$

and the distribution of the down quarks in the proton is the same as the distribution of the up quarks in the neutron:

$$d(x) \equiv d^p(x) = u^n(x). \tag{3.35}$$

If we also assume that different flavours (u, d, s) of the quarks occur with equal probability in the sea, then we can write down this total contribution S:

$$S \equiv u_s = \bar{u}_s = d_s = \bar{d}_s = s_s = \bar{s}_s. \tag{3.36}$$

So we can now write the proton and neutron structure functions in terms of the valence u in the proton and the valence d in the proton, and a sea quark contribution:

$$F_2^p(x) = x\left\{\frac{1}{9}\left[4u_v(x) + d_v(x)\right] + \frac{4}{3}S(x)\right\}, \tag{3.37}$$

$$F_2^n(x) = x\left\{\frac{1}{9}\left[4d_v(x) + u_v(x)\right] + \frac{4}{3}S(x)\right\}. \tag{3.38}$$

We expect that at small x ($x \ll 1$) the sea quarks should dominate, so that

$$\frac{F_2^n}{F_2^p} \to 1, \tag{3.39}$$

while at large x ($x \to 1$) the valence quarks should dominate (and $u_v(x) > d_v(x)$ since there are two up versus one down valence quarks in the proton), then

$$\frac{F_2^n}{F_2^p} \to \frac{1}{4}. \tag{3.40}$$

And this is exactly what is seen in DIS experiment results.

Recall the momentum sum rule:

$$\sum_i \int_0^1 dx\, x f_i(x) = 1, \tag{3.41}$$

but electron-proton DIS experiments find the light-quark contributions to be roughly

$$\int dx\, x[u(x) + \bar{u}(x)] \approx 0.36, \tag{3.42}$$

$$\int dx\, x[d(x) + \bar{d}(x)] \approx 0.18. \tag{3.43}$$

This tells us that almost half of the proton momentum is carried by electrically neutral partons. These experiments were repeated by using neutrino scattering, and they indicated that these neutral partons do not interact weakly (i.e. are not quarks), therefore the missing momentum has to be carried by gluons. The need for inclusion of gluons in the parton model is also evidenced by the scaling violations at finite Q^2 discussed in Sect. 3.2.2.

3.2.3 Neutron Beta Decay

We all know that free neutrons are unstable: they are stable inside nuclei, but if a neutron exists outside of the nucleus, then it has a lifetime of approximately 15 min. This is because it can decay to a proton by the weak interaction

$$n \to pe^{-}\bar{\nu}_e\,, \tag{3.44}$$

emitting a W boson which in turn decays into an electron and electron antineutrino.

Neutron decay is the simplest way of studying the weak interaction. The decay rate of the neutron is proportional to the matrix element of the weak $V-A$ current:

$$\begin{aligned}\langle p(p',s')|(V_\mu - A_\mu)|n(p,s)\rangle = \\ \bar{u}_p(p',s')\Big\{\gamma_\mu f_1(q^2) + i\frac{\sigma_{\mu\nu}q^\nu}{2M}f_2(q^2) + \frac{q_\mu}{2M}f_3(q^2) \\ -\left[\gamma_\mu\gamma_5 g_1(q^2) + i\frac{\sigma_{\mu\nu}q^\nu}{2M}\gamma_5 g_2(q^2) + \frac{q_\mu}{2M}\gamma_5 g_3(q^2)\right]\Big\}u_n(p,s).\end{aligned} \tag{3.45}$$

Because of the tiny mass difference between the proton and the neutron

$$M_n - M_p \simeq 1.3\ \text{MeV}\,, \tag{3.46}$$

the momentum transfer here is so small that all the terms proportional to q may be dropped, and we only need to consider to first order the contribution from the f_1 and g_1 terms. By convention, we call the value of f_1 at zero momentum g_V, and the corresponding value of g_1, g_A:

$$g_V = f_1(0), \quad g_A = g_1(0). \tag{3.47}$$

According to the conserved vector current (CVC) hypothesis, which says that the vector part of this weak $V-A$ current is the same as the vector part of the electromagnetic current, under isospin symmetry this $f_1(0)$, or g_V, will give us the charge of the system, which is one ($g_V = 1$). There also exists the so-called Adler-Weisberger relation which predicts $g_A = 1.26$. So how do we extract g_A from experiment? The decay rate for a neutron at rest and with spin pointing in the $\boldsymbol{s}_n$ direction is given by

$$\frac{dR}{dp_e d\Omega_e d\Omega_{\bar{\nu}}} = \frac{G_F^2|V_{ud}|^2}{(2\pi)^5}\left[\alpha + \beta\boldsymbol{v}_e\cdot\boldsymbol{v}_{\bar{\nu}} + \gamma\boldsymbol{s}_n\cdot\boldsymbol{v}_e + \delta\boldsymbol{s}_n\cdot\boldsymbol{v}_{\bar{\nu}}\right]p_e^2(E_{\max}-E_e)^2. \tag{3.48}$$

Here $\boldsymbol{v}_e$ and $\boldsymbol{v}_{\bar{\nu}}$ are the velocities of the final electron and electron antineutrino, respectively, G_F is Fermi constant, and V_{ud} is a CKM matrix element. E is the energy of the electron, p_e is the momentum of the electron, and $E_{\max}$ is the

difference between the neutron and proton masses, which provides a bound on the energy spectrum of the electron:

$$E_{\max} = M_n - M_p \simeq 1.3 \text{ MeV}. \tag{3.49}$$

So the decay rate is defined then in terms of the quantities α, β, γ and δ described as functions of g_V and g_A:

$$\begin{aligned} \alpha &= g_V^2 + 3g_A^2, & \beta &= g_V^2 - g_A^2, \\ \gamma &= 2(g_A g_V - g_A^2), & \delta &= 2(g_A g_V + g_V^2), \end{aligned} \tag{3.50}$$

allowing us to extract g_A from this experiment. We can see that even for an unpolarised neutron (in this case the γ and δ terms are zero, and we only have the α and β terms which are expressed in terms of squares of g_A and g_V), we can define $|g_A/g_V|$ through an accurate determination of the angular correlation between the outgoing electron and electron antineutrino. To determine the sign of g_A, spin-dependent measurements are required; in other words, we want at least one of the γ or δ terms to be nonzero since they are proportional to a single power of g_A. Current best determination of $|g_A/g_V|$ provided by Particle Data Group (PDG2012) gives $|g_A/g_V| = 1.2701(25)$.

3.2.3.1 Axial Form Factor

Considering the general case of the matrix element of the weak $V-A$ current, away from $q^2 = 0$, will give us access to the form factors as functions of q^2. If we consider only the axial-vector part of the weak current between the neutron and proton states from Eq. (3.45), we find

$$\begin{aligned} \langle p(p',s')|A^\mu(\boldsymbol{q})|n(p,s)\rangle = \bar{u}_p(p',s')\Big[&\gamma^\mu\gamma_5 G_A(q^2) + i\sigma^{\mu\nu}\gamma_5 \frac{q_\nu}{2M} G_T(q^2) \\ &+ \gamma_5 \frac{q^\mu}{2M} G_P(q^2)\Big] u_n(p,s). \end{aligned} \tag{3.51}$$

Similarly to Eq. (3.10) for electromagnetic form factors, this is written in terms of Lorentz invariant form factors. The first term, which we call now $G_A(q^2)$, is the axial form factor, the third term, $G_P(q^2)$, is the induced pseudoscalar form factor, and the second term, the tensor form factor G_T, vanishes if charge symmetry assumed, $u_p = d_n$. The partially conserved axial current relation (PCAC) tells us that the divergence of the matrix element of the axial-vector current is proportional to m_π^2 which, as we go to chiral limit, should vanish:

$$\partial_\mu A^\mu \propto m_\pi^2 \xrightarrow{m_q \to 0} 0\,, \tag{3.52}$$

i.e. the axial current is only conserved in the chiral limit. This is, in general, not true for Eq. (3.51). However if G_P has a pion pole

$$G_P(q^2) \to \frac{4M_N f_\pi g_{\pi NN}(q^2)}{-q^2 + m_\pi^2}, \tag{3.53}$$

and G_A takes the following form in terms of $g_{\pi NN}$ and the pion decay constant f_π

$$M_N G_A(q^2) = f_\pi g_{\pi NN}(q^2), \tag{3.54}$$

then the matrix element in Eq. (3.51) satisfies the PCAC relation. Then at $q^2 = 0$ we get the so-called Goldberger-Treiman relation

$$M_N g_A = f_\pi g_{\pi NN}. \tag{3.55}$$

3.2.3.2 Axial Charge g_A

As discussed above, the axial charge is defined as the value of the axial form factor at $q^2 = 0$, $g_A = G_A(q^2 = 0)$. This presents an ideal quantity for benchmark lattice calculations of nucleon structure. The fact that it is defined at zero momentum guarantees that calculations are statistically clean. This is also an isovector quantity since this matrix element between the proton and neutron with a $\bar{u}d$ current is related under charge symmetry to the $u - d$ proton matrix element

$$\langle p|\bar{u}\gamma^\mu\gamma^5 d|n\rangle = \langle p|\bar{u}\gamma^\mu\gamma^5 u - \bar{d}\gamma^\mu\gamma^5 d|p\rangle, \tag{3.56}$$

and therefore, disconnected contributions cancel. So in principle it should be possible to perform precision lattice calculations of g_A which can be compared to the experimental value.

3.3 Determining Matrix Elements on the Lattice

Here we outline the procedure required for calculating matrix elements such as those in Eqs. (3.51) and (3.10). We start with introducing lattice three-point functions and the sequential-source technique used for calculating them. We then show how to extract the relevant matrix elements from these three-point functions through constructing ratios of lattice three- and two-point functions.

3.3.1 Lattice Three-Point Functions

We start our discussion by introducing the lattice nucleon three-point function

$$G(t,\tau;p,p') = \sum_{\boldsymbol{x_2},\boldsymbol{x_1}} e^{-i\,\boldsymbol{p'}\cdot(\boldsymbol{x_2}-\boldsymbol{x_1})} e^{-i\,\boldsymbol{p}\cdot\boldsymbol{x_1}} \Gamma_{\beta\alpha} \cdot \\ \cdot \langle \Omega | T\{\chi_\alpha(\boldsymbol{x_2},t)\mathcal{O}(\boldsymbol{x_1},\tau)\bar{\chi}_\beta(0)\}|\Omega\rangle\,, \tag{3.57}$$

which is also illustrated in Fig. 3.8, where a particle is created at $t = 0$ by the creation operator $\bar{\chi}_\beta(0)$, interacts with the generic current $\mathcal{O}(\boldsymbol{x_1},\tau)$ at some Euclidean time τ and is annihilated at some time t by the annihilation operator $\chi_\alpha(\boldsymbol{x_2},t)$. In our case the creation (annihilation) operator has the quantum numbers of the proton. A time-ordered product ensures that everything happens in correct order. The $\Gamma_{\beta\alpha}$ matrix is the spin-projection operator, Ω represents the vacuum state and, finally, the Fourier transform projects the particle to a definite momentum state. Inserting a complete set of states $I = \sum_{B^{(\prime)},p^{(\prime)},s^{(\prime)}} |B^{(\prime)},p^{(\prime)},s^{(\prime)}\rangle\langle B^{(\prime)},p^{(\prime)},s^{(\prime)}|$ before and after the current operator and exploiting the translational invariance $\chi(\boldsymbol{x},t) = e^{\hat{H}t} e^{-i\,\hat{\boldsymbol{P}}\cdot\boldsymbol{x}} \chi(0) e^{i\,\hat{\boldsymbol{P}}\cdot\boldsymbol{x}} e^{-\hat{H}t}$, we find

$$G(t,\tau;p,p') = \sum_{B,B'}\sum_{s,s'} e^{-E_{B'}(\boldsymbol{p'})(t-\tau)} e^{-E_B(\boldsymbol{p})\tau} \Gamma_{\beta\alpha} \times \\ \left\langle \Omega \left| \chi_\alpha(0) \right| B',p',s' \right\rangle \left\langle B',p',s' \left| \mathcal{O}(\boldsymbol{q}) \right| B,p,s \right\rangle \left\langle B,p,s \left| \bar{\chi}_\beta(0) \right| \Omega \right\rangle\,, \tag{3.58}$$

where $E_B(\boldsymbol{p})$ denotes the energy of the baryon B with momentum $\boldsymbol{p}$. As the Euclidean time evolves, $0 \ll \tau \ll t$, excited states are exponentially suppressed and the ground-state proton dominates

$$G(t,\tau;p,p') = \sum_{s,s'} e^{-E_{p'}(t-\tau)} e^{-E_p\tau} \Gamma_{\beta\alpha} \times \\ \left\langle \Omega \left| \chi_\alpha(0) \right| N(p',s') \right\rangle \left\langle N(p',s') \left| \mathcal{O}(\boldsymbol{q}) \right| N(p,s) \right\rangle \left\langle N(p,s) \right| \bar{\chi}_\beta(0) \left| \Omega \right\rangle\,, \tag{3.59}$$

where we have simplified our notation and E_p now denotes the energy of the proton with momentum $p = |\boldsymbol{p}|$.

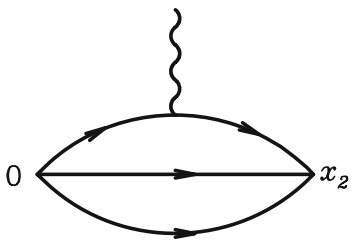

Fig. 3.8 Quark-flow diagram for a proton three-point function described in Eq. (3.57)

3.3.1.1 Three-Point Functions at the Quark Level

We now wish to derive a form for a lattice three-point function in terms of quark propagators. We will start with the simple case of the pion for which we will use the standard interpolating operator

$$\chi(x) = \bar{d}(x)\gamma_5 u(x), \tag{3.60}$$

where $\bar{d}(x)$ and $u(x)$ are the quark fields and γ_5 gives the correct quantum numbers for a pseudoscalar meson. Inserting the local current operator,

$$\mathcal{O}(x) = \bar{q}(x)\Gamma q(x), \tag{3.61}$$

where Γ stands for any combination of γ-matrices and derivatives (e.g. γ_μ for the electromagnetic current), the three-point function of pion is then

$$\begin{aligned} G(t,\tau;p,p') = \sum_{\boldsymbol{x_2},\boldsymbol{x_1}} & e^{-i\,\boldsymbol{p'}\cdot(\boldsymbol{x_2}-\boldsymbol{x_1})} e^{-i\,\boldsymbol{p}\cdot\boldsymbol{x_1}} \\ & \left\langle \Omega \left| T\left\{ -\bar{d}(x_2)\gamma_5 u(x_2)\bar{u}(x_1)\Gamma u(x_1)\bar{u}(0)\gamma_5 d(0)\right\}\right| \Omega\right\rangle , \end{aligned} \tag{3.62}$$

where we are first considering the u-quark contribution to the full three-point function. Writing the colour (Latin) and Dirac (Greek) indices explicitly,

$$\begin{aligned} G(t,\tau;p,p') = & \sum_{\boldsymbol{x_2},\boldsymbol{x_1}} e^{-i\,\boldsymbol{p'}\cdot(\boldsymbol{x_2}-\boldsymbol{x_1})} e^{-i\,\boldsymbol{p}\cdot\boldsymbol{x_1}} \times \\ & \left\langle \Omega | T\{ -\bar{d}^a_\beta(x_2)\gamma^5_{\beta\gamma} u^a_\gamma(x_2)\bar{u}^b_\rho(x_1)\Gamma_{\rho\delta} u^b_\delta(x_1)\bar{u}^c_\xi(0)\gamma^5_{\xi\alpha} d^c_\alpha(0)\} | \Omega \right\rangle, \end{aligned} \tag{3.63}$$

we now perform all possible Wick contractions,

$$\begin{aligned} G(t,\tau;p,p') = & \sum_{\boldsymbol{x_2},\boldsymbol{x_1}} e^{-i\,\boldsymbol{p'}\cdot(\boldsymbol{x_2}-\boldsymbol{x_1})} e^{-i\,\boldsymbol{p}\cdot\boldsymbol{x_1}} \times \\ & \left\{ S^{ca}_{d\alpha\beta}(0,x_2)\gamma^5_{\beta\gamma} S^{ab}_{u\gamma\rho}(x_2,x_1)\Gamma_{\rho\delta} S^{bc}_{u\delta\xi}(x_1,0)\gamma^5_{\xi\alpha} \right. \\ & \left. - S^{ca}_{d\alpha\beta}(0,x_2)\gamma^5_{\beta\gamma} S^{ac}_{u\gamma\xi}(x_2,0)\gamma^5_{\xi\alpha} S^{bb}_{u\delta\rho}(x_1,x_1)\Gamma_{\rho\delta} \right\}, \end{aligned} \tag{3.64}$$

where S_q stands for the quark propagator. Then we take the Dirac and colour traces to obtain

$$\begin{aligned} G(t,\tau;p,p') = & \sum_{\boldsymbol{x_2},\boldsymbol{x_1}} e^{-i\,\boldsymbol{p'}\cdot(\boldsymbol{x_2}-\boldsymbol{x_1})} e^{-i\,\boldsymbol{p}\cdot\boldsymbol{x_1}} \\ & \left\{ \mathrm{Tr}[S_d(0,x_2)\gamma_5 S_u(x_2,x_1)\Gamma S_u(x_1,0)\gamma_5] \right. \\ & \left. - \mathrm{Tr}[S_d(0,x_2)\gamma_5 S_u(x_2,0)\gamma_5]\,\mathrm{Tr}[S_u(x_1,x_1)\Gamma] \right\}, \end{aligned} \tag{3.65}$$

and using the γ_5-hermiticity, $S^\dagger(x,0) = \gamma_5 S(0,x)\gamma_5$, we end up with

$$\begin{aligned} G(t,\tau;p,p') = \sum_{\boldsymbol{x_2},\boldsymbol{x_1}} & e^{-i\,\boldsymbol{p'}\cdot(\boldsymbol{x_2}-\boldsymbol{x_1})} e^{-i\,\boldsymbol{p}\cdot\boldsymbol{x_1}} \\ & \Big\{ \mathrm{Tr}[S_d^\dagger(x_2,0) S_u(x_2,x_1) \Gamma S_u(x_1,0)] \\ & - \mathrm{Tr}[S_d^\dagger(x_2,0) S_u(x_2,0)]\,\mathrm{Tr}[S_u(x_1,x_1)\Gamma] \Big\} . \end{aligned} \tag{3.66}$$

We can a similar result for the d-quark contribution $\bar{d}\,\Gamma\, d$, which, however, in the isospin limit is identical to that for the u-quark. The first term of Eq. (3.66) stands for the usual connected diagram whereas the $S_u(x_1,x_1)$ in second term indicates a quark loop and a disconnected diagram.

So in this case we have found that there are two dominant terms needed to calculate the full pion three-point function; however, due to the number of quark fields, it gets complicated when we consider the proton.

The interpolating operator of proton is

$$\chi_\alpha(x) = \epsilon^{abc} \left(u^{Ta}(x) C\gamma_5 d^b(x)\right) u^c_\alpha(x) , \tag{3.67}$$

leading to the three-point function for, e.g., the u-quark current insertion,

$$\begin{aligned} G_\Gamma(t,\tau;p,p') = & \sum_{\boldsymbol{x_2},\boldsymbol{x_1}} e^{-i\,\boldsymbol{p'}\cdot(\boldsymbol{x_2}-\boldsymbol{x_1})} e^{-i\,\boldsymbol{p}\cdot\boldsymbol{x_1}} \Gamma \epsilon^{abc} \epsilon^{a'b'c'} \times \\ & \Big\langle \Omega \Big| T \Big\{ \Big(u^{Ta}(x_2) C\gamma_5 d^b(x_2)\Big) u^c_\alpha(x_2) \bar{u}(x_1) \mathcal{O} u(x_1) \bar{u}^{c'}(0) \cdot \\ & \Big(\bar{d}^{b'}(0) C\gamma_5 \bar{u}^{Ta'}(0)\Big) \Big\} \Big| \Omega \Big\rangle , \end{aligned} \tag{3.68}$$

where C is the charge-conjugation operator. After all possible connected Wick contractions we can write this three-point function in terms of up and down pieces,

$$G_\Gamma(t,\tau;p,p') = q_u C^u_\Gamma(t,\tau;p,p') + q_d C^d_\Gamma(t,\tau;p,p'), \tag{3.69}$$

where for the electromagnetic current we have explicitly included the electric charges of the up and down quarks ($q_{u,d}$), and $C^u_\Gamma(t,\tau;p,p')$ and $C^d_\Gamma(t,\tau;p,p')$ are defined as

$$\begin{aligned} C^{u,d}_\Gamma(t,\tau;p,p') \equiv & \sum_{\boldsymbol{x_1}} e^{-i\,\boldsymbol{q}\cdot\boldsymbol{x_1}} \times \\ & \Big\langle \mathrm{Tr}\Big[\Sigma^{u,d}_\Gamma(\boldsymbol{0},0;\boldsymbol{x_1},\tau;\boldsymbol{p'},t) \mathcal{O}(\boldsymbol{x_1},\tau) S(\boldsymbol{x_1},\tau;0) \Big] \Big\rangle , \end{aligned} \tag{3.70}$$

where $\boldsymbol{q} = \boldsymbol{p}' - \boldsymbol{p}$ is the momentum transfer. The $\Sigma_\Gamma^{u,d}$ term is the combination of propagators shown in Fig. 3.9 and written as

$$\Sigma_\Gamma^{u,d}(\mathbf{0}, 0; \boldsymbol{x_1}, \tau; \boldsymbol{p}', t) = \sum_{\boldsymbol{x_2}} S_\Gamma^{u,d}(\boldsymbol{x_2}, t; \mathbf{0}, 0; \boldsymbol{p}') S(\boldsymbol{x_2}, t; \boldsymbol{x_1}, \tau), \tag{3.71}$$

where S_Γ^u and S_Γ^d are

$$\begin{aligned} S_\Gamma^{u;a'a}(\boldsymbol{x_2}, t; \mathbf{0}, 0; \boldsymbol{p}') &= e^{-i\,\boldsymbol{p}'\cdot\boldsymbol{x_2}} \epsilon^{abc} \epsilon^{a'b'c'} \times \\ &\Big\{ \tilde{S}^{d;bb'}(\boldsymbol{x_2}, t; \mathbf{0}, 0) S^{u;cc'}(\boldsymbol{x_2}, t; \mathbf{0}, 0) \Gamma \\ &+ \mathrm{Tr_D}\left[\tilde{S}^{d;bb'}(\boldsymbol{x_2}, t; \mathbf{0}, 0) S^{u;cc'}(\boldsymbol{x_2}, t; \mathbf{0}, 0) \right] \Gamma \\ &+ \Gamma S^{u;bb'}(\boldsymbol{x_2}, t; \mathbf{0}, 0) \tilde{S}^{d;cc'}(\boldsymbol{x_2}, t; \mathbf{0}, 0) \\ &+ \mathrm{Tr_D}\left[\Gamma S^{u;bb'}(\boldsymbol{x_2}, t; \mathbf{0}, 0) \right] \tilde{S}^{d;cc'}(\boldsymbol{x_2}, t; \mathbf{0}, 0) \Big\}, \end{aligned} \tag{3.72}$$

$$\begin{aligned} S_\Gamma^{d;a'a}(\boldsymbol{x_2}, t; \mathbf{0}, 0; \boldsymbol{p}') &= e^{-i\,\boldsymbol{p}'\cdot\boldsymbol{x_2}} \epsilon^{abc} \epsilon^{a'b'c'} \times \\ &\Big\{ \tilde{S}^{u;bb'}(\boldsymbol{x_2}, t; \mathbf{0}, 0) \tilde{\Gamma} \tilde{S}^{u;cc'}(\boldsymbol{x_2}, t; \mathbf{0}, 0) \\ &+ \mathrm{Tr_D}\left[\Gamma S^{u;bb'}(\boldsymbol{x_2}, t; \mathbf{0}, 0) \right] \tilde{S}^{u;cc'}(\boldsymbol{x_2}, t; \mathbf{0}, 0) \Big\}, \end{aligned} \tag{3.73}$$

and we have defined $\tilde{S} \equiv C\gamma_5 S \gamma_5 C$. We also note that $\mathrm{Tr_D}$ indicates a trace of Dirac indices, while the colour indices are still explicit.

Now that we have expressed the three-point function in terms of quark propagators, we can calculate it by computing and contracting the propagators. However, because of the $S(\boldsymbol{x_2}, t; \boldsymbol{x_1}, \tau)$ propagator and the presence of sums over $\boldsymbol{x_1}$, $\boldsymbol{x_2}$ we can not calculate the quantities given in Eq. (3.70) directly. The workaround is to use the sequential-source technique in which we first compute the ordinary propagators $S(x, 0)$ and then construct the sources $S_\Gamma^{u;a'a}$ or $S_\Gamma^{d;a'a}$, as described in Eqs. (3.72)

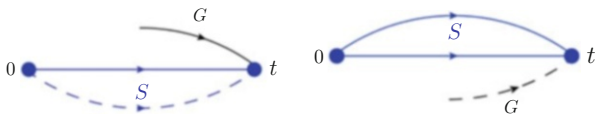

Fig. 3.9 Diagrammatic view of the Σ_Γ term for up (*left*) and down (*right*) quark contributions. The blue S combination corresponds to the $S_\Gamma^{u,d}(\boldsymbol{x_2}, t; \mathbf{0}, 0; \boldsymbol{p}')$ piece and the black G stands for $S(\boldsymbol{x_2}, t; \boldsymbol{x_1}, \tau)$. *Solid (dashed) lines* indicate $u(d)$-quark propagators

and (3.73). The sequential propagator $\Sigma_{\Gamma}^{u,d}(\mathbf{0}, 0; \boldsymbol{x_1}, \tau; \boldsymbol{p}', t)$ is then computed via a second inversion by solving the linear system of equations

$$\sum_{x_1} M(x_2, x_1)\gamma_5 \Sigma_{\Gamma}^{\dagger u,d}(\mathbf{0}, 0; \boldsymbol{x_1}, \tau; \boldsymbol{p}', t) = \gamma_5 S_{\Gamma}^{\dagger u,d}(\boldsymbol{x_2}, t; \mathbf{0}, 0; \boldsymbol{p}'). \tag{3.74}$$

Contracting the sequential propagator with the operator $\mathcal{O}(\boldsymbol{x_1}, \tau)$ and an ordinary propagator from source to current $S(\boldsymbol{x_1}, 0)$, we can construct the three-point function as in Eq. (3.70).

With this approach we have inverted the sequential propagator through the sink by fixing the final-state particle and sink momentum. This allows us to investigate the momentum dependence of the form factors for different insertion currents, since the sum over $\boldsymbol{x_1}$ is performed last. Alternatively, we could have chosen to invert the sequential source through the current, leaving the choice of final-state particle free; however, we would need separate a inversion for each choice of $\boldsymbol{q}$ and operator. The advantage of this method, however, is that the choice of quark sector, hadron boost and polarisation are all free to be determined after the sequential propagator has been calculated. Further information can be found in [142]. Choosing between these two approaches depends on what we are interested in computing. Mapping out the q^2-dependence of various form factors for a single hadronic state would be suited to choosing the "sequential source through the sink" method, as described in Eqs. (3.70)–(3.74), while comparing results for a single operator for a number of different hadronic states would be more suited to the "sequential source through the current method".

3.3.2 Extracting Matrix Elements

Recall the nucleon three-point function given in Eq. (3.57). Since we are interested in determining the matrix element $\langle N(p', s') | \mathcal{O}(\boldsymbol{q}) | N(p, s) \rangle$, we should somehow cancel the exponential time-dependent factors and wavefunction amplitudes, i.e. $\langle \Omega | \chi_\alpha(0) | N(p', s') \rangle$ and $\langle N(p, s) | \bar{\chi}_\beta(0) | \Omega \rangle$, which are, in general, momentum dependent. For this purpose we will use the nucleon two-point function,

$$G_2(t, \boldsymbol{p}) = \sum_s e^{-E_p t} \Gamma_{\beta\alpha} \langle \Omega | \chi_\alpha | N(p, s) \rangle \left\langle N(p, s) \left| \bar{\chi}_\beta \right| \Omega \right\rangle, \tag{3.75}$$

and consider the combination of the nucleon three- and two-point functions

$$R(t, \tau; \boldsymbol{p}', \boldsymbol{p}; \mathcal{O}) = \frac{G_\Gamma(t, \tau; \boldsymbol{p}', \boldsymbol{p}; \mathcal{O})}{G_2(t, \boldsymbol{p}')} \left[\frac{G_2(\tau, \boldsymbol{p}') G_2(t, \boldsymbol{p}') G_2(t - \tau, \boldsymbol{p})}{G_2(\tau, \boldsymbol{p}) G_2(t, \boldsymbol{p}) G_2(t - \tau, \boldsymbol{p}')} \right]^{\frac{1}{2}}. \tag{3.76}$$

With periodic or anti-periodic boundary conditions in time, the two-point function in Eq. (3.75) can be written in terms of nucleon spinors

$$G_2(t,\boldsymbol{p}) = \sum_s \frac{\sqrt{Z^{\text{snk}}(\boldsymbol{p})\bar{Z}^{\text{src}}(\boldsymbol{p})}}{2E_{\boldsymbol{p}}} \text{Tr}\left[\bar{u}(\boldsymbol{p},s)\Gamma u(\boldsymbol{p},s)\right]\left[e^{-E_p t} + e^{-E'_p(T-t)}\right] + \nu\text{-spinor terms with opposite parity,} \tag{3.77}$$

where the $Z^{\text{src(snk)}}$ is the wavefunction overlap with the proton at the source (sink) and T is the lattice time extent. Using the relation for spinors in Euclidean space

$$\sum_s u(\boldsymbol{p},s)\bar{u}(\boldsymbol{p},s) = -i\not{p} + m\ , \tag{3.78}$$

together with the projection matrix $\Gamma_4 = (1+\gamma_4)/2$, to maximise the overlap with the positive-parity forward-propagating state we get

$$G_2(t,\boldsymbol{p}) = \sqrt{Z^{\text{snk}}(\boldsymbol{p})\bar{Z}^{\text{src}}(\boldsymbol{p})}\left[\left(\frac{E_p+m}{E_p}\right)e^{-E_p t} + \left(\frac{E'_p+m'}{E'_p}\right)e^{-E'_p(T-t)}\right]. \tag{3.79}$$

Similarly, for the three-point function, when $0 \ll \tau \ll t \ll \frac{1}{2}T$, we get

$$G_\Gamma(t,\tau;\boldsymbol{p}',\boldsymbol{p};\mathcal{O}) = \sqrt{Z^{\text{snk}}(\boldsymbol{p}')\bar{Z}^{\text{src}}(\boldsymbol{p})}F(\Gamma,\mathcal{J})e^{-E_{p'}(t-\tau)}e^{-E_p\tau}, \tag{3.80}$$

where

$$F(\Gamma,\mathcal{J}) = \frac{1}{4}\text{Tr}\left[\left(\gamma_4 - i\frac{\boldsymbol{p}'\cdot\boldsymbol{\gamma}}{E_{p'}} + \frac{m}{E_{p'}}\right)\mathcal{J}\left(\gamma_4 - i\frac{\boldsymbol{p}\cdot\boldsymbol{\gamma}}{E_p} + \frac{m}{E_p}\right)\right]. \tag{3.81}$$

The nucleon matrix elements we are interested in will now have the form

$$\langle N(p',s')|\mathcal{O}(\boldsymbol{q})|N(p,s)\rangle = \bar{u}(p',s')\mathcal{J}u(p,s), \tag{3.82}$$

where we have labeled the combination of gamma matrices and Lorentz-invariant form factors sandwiched between two nucleon spinors generically as $\mathcal{J}$. For example, for the electromagnetic current we have

$$\mathcal{J} = \gamma^\mu F_1(Q^2) + i\sigma^{\mu\nu}\frac{q_\nu}{2M}F_2(Q^2)\ . \tag{3.83}$$

3.3.2.1 Example 1: Form Factors

As an example, if we choose the unpolarised projection matrix Γ_4, the electromagnetic current as our operator, and $\boldsymbol{p} = \boldsymbol{p}' = \mathbf{0}$, then the term proportional to $F_2(Q^2)$ in Eq. (3.83) vanishes and we have

$$\langle N(p',s')|J^{\mu}(0)|N(p,s)\rangle = \bar{u}(p',s')\gamma^{\mu}u(p,s)F_1(Q^2=0)\,. \tag{3.84}$$

Hence we are in a position to determine $F_1(Q^2 = 0)$.

First of all, we should remember that this matrix element is defined in Minkowski space while we work in Euclidean space, so we need to Euclideanise it using relations for transforming Minkowski gamma matrices to Euclidean gamma matrices, and we also need to transform our momenta:

$$\gamma_0^M = \gamma_4^E, \quad \gamma_i^M = -i\,\gamma_i^E, \quad p_4^E = ip_0^M \equiv iE(\boldsymbol{p}), \quad p_i^E = -p_i^M\,. \tag{3.85}$$

After Euclideanisation we can see that the matrix element (3.10) can be written in the form

$$\begin{aligned}\langle N(p',s')|\bar{q}\gamma_{\mu}^E q|N(p,s)\rangle = \bar{u}(p',s')\gamma_{\mu}^E u(p,s)F_1(Q^2) \\ +\bar{u}(p',s')\frac{\sigma_{\mu\nu}^E q_{\nu}^E}{2M}u(p,s)F_2(Q^2),\end{aligned} \tag{3.86}$$

which looks very similar to Eq. (3.10), except for a factor of i in the second term. Recalling that in our current example $q_{\nu}^E = 0$, we can rewrite this as

$$\langle N(p',s')|\bar{q}\gamma_{\mu}^E q|N(p,s)\rangle = \bar{u}(p',s')\gamma_{\mu}^E u(p,s)F_1(Q^2=0)\,, \tag{3.87}$$

and Eq. (3.83) reduces to

$$\mathcal{J} = \gamma^{\mu}F_1(Q^2=0)\,, \tag{3.88}$$

which we can substitute into Eq. (3.81). If we insert the time component and the spatial components of the vector of gamma matrices separately, we will get (after taking the trace) the following:

$$F(\Gamma_4,\gamma_4) = \frac{1}{2E_{\boldsymbol{p}}E_{\boldsymbol{p}'}}\left[(E_{\boldsymbol{p}}+m)(E_{\boldsymbol{p}'}+m)+\boldsymbol{p}'\cdot\boldsymbol{p}\right]\,, \tag{3.89}$$

$$F(\Gamma_4,\gamma_i) = \frac{-i}{2E_{\boldsymbol{p}}E_{\boldsymbol{p}'}}\left[(E_{\boldsymbol{p}}+m)\boldsymbol{p}'+(E_{\boldsymbol{p}'}+m)\boldsymbol{p}\right]. \tag{3.90}$$

If we now take the specific case relevant to our example where both source and sink momenta are zero ($\boldsymbol{p}' = \boldsymbol{p} = 0$), then we will get

$$F(\Gamma_4, \gamma_4) = 2\, F_1(Q^2 = 0)\,, \tag{3.91}$$

while the spatial components vanish

$$F(\Gamma_4, \gamma_i) = 0\,. \tag{3.92}$$

Now we can go back to the ratio of three- and two-point functions (Eq. (3.76)) and, after working it through, we will find that it simply provides the factor $\sqrt{\frac{E_{p'}E_p}{(E_{p'}+m)(E_p+m)}}$ in terms of energies and mass, times the function $F(\Gamma, \mathcal{J}(\boldsymbol{q}))$:

$$R(t, \tau; \boldsymbol{p}', \boldsymbol{p}; \mathcal{O}) = \sqrt{\frac{E_{p'}E_p}{(E_{p'}+m)(E_p+m)}} F(\Gamma, \mathcal{J}(\boldsymbol{q})) \quad \left\{ 0 \ll \tau \ll t \ll \frac{1}{2}T \right\}. \tag{3.93}$$

And if we look, again, at our very specific case:

$$\Gamma_4 = \frac{1}{2}(1+\gamma_4), \quad \mathcal{O} = V_4 \equiv \gamma_4, \quad \boldsymbol{p}' = \boldsymbol{p} = 0, \tag{3.94}$$

then the ratio in Eq. (3.93) will give us directly F_1 at $Q^2 = 0$:

$$R(t, \tau; \boldsymbol{p}', \boldsymbol{p}; \mathcal{O}) = F_1(q^2 = 0). \tag{3.95}$$

We can also choose certain combinations of parameters and kinematics which provide access to the Sachs form factors,

$$R(t, \tau; 0, \boldsymbol{p}; \gamma_4, \Gamma_4) = K \left(F_1(q^2) - \frac{E_p - M}{2M} F_2(q^2) \right) = K\, G_E(q^2), \tag{3.96}$$

$$R(t, \tau; 0, \boldsymbol{p}; \gamma_i, \Gamma_4) = -iK \frac{q_i}{E_p + M} G_E(q^2), \tag{3.97}$$

$$R(t, \tau; 0, \boldsymbol{p}; \gamma_i, \Gamma_j) = -iK\epsilon_{ijk} \frac{q_k}{E_p + M} G_M(q^2), \tag{3.98}$$

where $K = \sqrt{(E_p + M)/(2E_p)}$ and $\Gamma_j = i(1+\gamma_4)\gamma_5\gamma_j/2$. In Fig. 3.10 we show some results from [143] for the ratio in Eq. (3.96) for several choices of momentum transfer. As we can clearly see, the ratio decreases in size as we increase the momentum transfer, indicating that the form factor $G_E(q^2)$ falls as a function of q^2.

More generally, we can consider all combinations that contribute at a fixed q^2, construct a set of simultaneous equations and solve for the two unknowns, $F_1(q^2)$

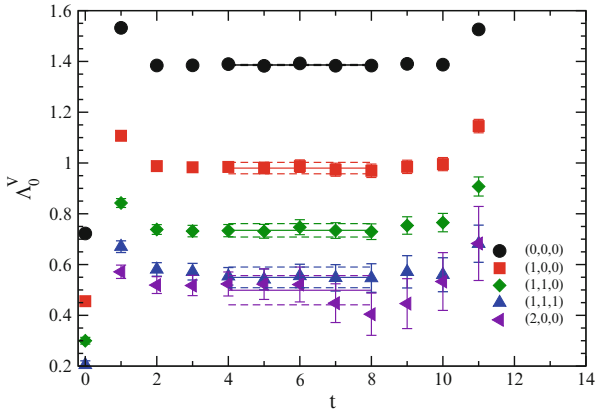

Fig. 3.10 Ratio of three- and two-point functions from Eq. (3.96) from [143]

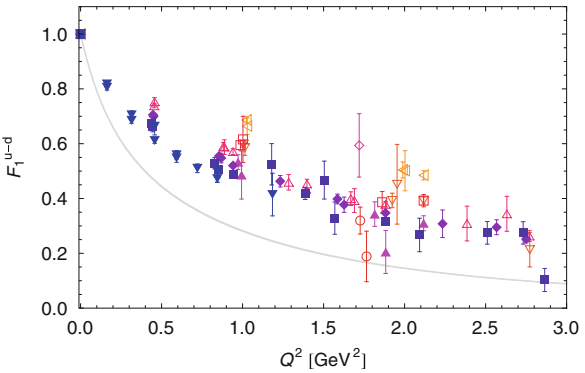

Fig. 3.11 $F_1^{(u-d)}(q^2)$ for several values of 250 MeV $< m_\pi <$ 1.5 GeV from [144]

and $F_2(q^2)$. As an example, we show in Fig. 3.11 some lattice results for $F_1(q^2)$ from [144] for a range of pion masses 250 MeV $< m_\pi <$ 1.5 GeV compared to a parameterisation of experimental data denoted by the shaded band [145]. As can be seen, the lattice results lie above the experimental band, although this is now known to be due to the large pion masses used in many lattice simulations [146].

3.3.2.2 Example 2: g_A

In order to compute the nucleon axial charge, g_A, we need access to the matrix element given in Eq. (3.51) in the forward ($q^2 = 0$) limit,

$$\langle p|\bar{u}\gamma^\mu\gamma^5 d|n\rangle = \bar{u}(p',s')\gamma^\mu\gamma^5 u(p,s)g_A\,. \tag{3.99}$$

As we did in the previous section for the electromagnetic form factors, we wish to isolate this matrix element from the lattice three-point function (Eq. (3.57)). In other words, we wish to determine the matrix element Eq. (3.82) for the particular case where the operator $\mathcal{O}$ is the axial current and the Dirac structure on the right-hand side of Eq. (3.99) shows that in this particular case $\mathcal{J}$ in Eq. (3.82) is simply

$$\mathcal{J} = \gamma_\mu \gamma_5 \, g_A \, . \tag{3.100}$$

We can now substitute this into $F(\Gamma, \mathcal{J})$ defined in Eq. (3.81). For unpolarised gamma nucleons, i.e. $\Gamma = \Gamma_{\text{unpol}}$, we find

$$F(\Gamma_{\text{unpol}}, \gamma_4\gamma_5) = 0, \quad F(\Gamma_{\text{unpol}}, \gamma_i\gamma_5) = 0. \tag{3.101}$$

Obviously, we need a different choice of projection matrix. In order to polarise our nucleon states so that they have definite spin in a particular direction $\boldsymbol{s}$, we will need to use the spin-projectors

$$\Gamma_{\text{pol}} = \frac{1}{2}(1+\gamma_4) i\gamma_5 \boldsymbol{\gamma}\cdot\boldsymbol{s} \, . \tag{3.102}$$

Re-evaluating $F(\Gamma, \mathcal{J})$ in Eq. (3.81) with this choice, we find for time and spatial components of the axial current

$$F(\Gamma_{\text{pol}}, \gamma_4\gamma_5) = -\frac{1}{2E_{\boldsymbol{p}}E_{\boldsymbol{p}'}}\left[(E_{\boldsymbol{p}}+m)\boldsymbol{p}'\cdot\boldsymbol{s} + (E_{\boldsymbol{p}'}+m)\boldsymbol{p}\cdot\boldsymbol{s}\right], \tag{3.103}$$

$$F(\Gamma_{\text{pol}}, \gamma_i\gamma_5) = \frac{i}{2E_{\boldsymbol{p}}E_{\boldsymbol{p}'}}\left[(E_{\boldsymbol{p}}+m)(E_{\boldsymbol{p}'}+m)\boldsymbol{s} + \right. \tag{3.104}$$

$$\left. (\boldsymbol{p}'\cdot\boldsymbol{s})\boldsymbol{p} + (\boldsymbol{p}\cdot\boldsymbol{s})\boldsymbol{p}' - (\boldsymbol{p}'\cdot\boldsymbol{p})\boldsymbol{s}\right]_i \, ,$$

which now depend not only on the energy and momenta of the nucleon states, but also on the direction of its spin.

In particular, we notice that for the spatial component (Eq. (3.104)) we have terms that are proportional directly to $\boldsymbol{p}$ and $\boldsymbol{p}'$, but there is also a term $(E_{\boldsymbol{p}} + m)(E_{\boldsymbol{p}'} + m)\boldsymbol{s}$ which is not proportional to momentum but proportional to the nucleon's energy and the direction of its spin. So even in the case when both $\boldsymbol{p}$ and $\boldsymbol{p}'$ are zero we have a nonzero contribution

$$F(\Gamma_{\text{pol}}, \gamma_i\gamma_5) = 2i s_i, \tag{3.105}$$

and g_A can be determined by choosing the direction of axial current to be the same as the direction of nucleon polarisation. For example, if we choose the polarisation of the nucleon to be in the z-direction, then we need to compute lattice three-point functions with

$$\Gamma_{\text{pol}} = \Gamma_3 = \frac{1}{2}(1+\gamma_4) i\gamma_5\gamma_3, \quad \mathcal{O} = \bar{q}\gamma_3\gamma_5 q \, . \tag{3.106}$$

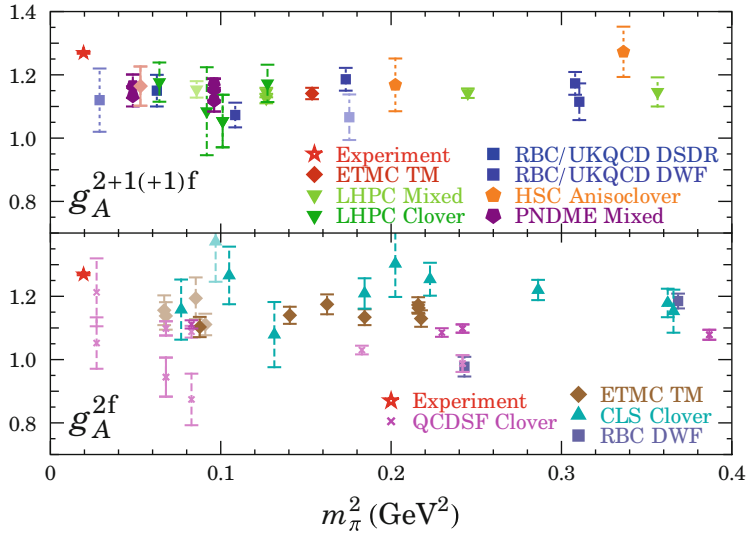

Fig. 3.12 Summary of lattice calculations of g_A by H.-W. Lin [147]

With these particular choice of kinematics ($\boldsymbol{p} = \boldsymbol{p}' = \mathbf{0}$), the ratio defined in Eq. (3.76) simplifies to provide a direct determination of g_A

$$R(t,\tau;\mathbf{0},\mathbf{0};\gamma_3\gamma_5,\Gamma_3) = \frac{G_{\Gamma_3}(t,\tau;\mathbf{0},\mathbf{0};\gamma_3\gamma_5)}{G_2(t,\mathbf{0})} = ig_A\,, \tag{3.107}$$

Due to its status as a benchmark calculation for nucleon structure simulations, g_A has been heavily investigated on the lattice. In Fig. 3.12 we show a summary of calculations by several lattice collaborations compiled by H.-W. Lin [147] in 2012. It is clear that there is broad agreement between the many different groups, with the bulk of the results lying about 10 % below the experimental value. This discrepancy has attracted much attention recently with several arguments such as excited state contamination [148] and finite volumes effects [149] being put forward as explanations. We will not go into a discussion regarding these issues here.

3.3.3 Moments of Structure Functions

In order to proceed towards lattice calculations of matrix elements relevant to structure functions, we need to consider what is called the moments of the structure functions. Moments are integrals with respect to the momentum fraction x, weighted with some power of x, and as we increase this power, this increases the moment, e.g.

$$\int_0^1 dx\, x^{n-2} F_2(x, Q^2) = E^{\mathcal{S}}_{F_2;\nu_n}(M^2/Q^2, g^{\mathcal{S}}) \nu_n^{\mathcal{S}}(M) + \mathcal{O}(1/Q^2). \tag{3.108}$$

These moments can be separated at some renormalisation scale M in a scheme $\mathcal{S}$ into a perturbative part, which is called a Wilson coefficient (E) and calculable in perturbation theory, and a nonperturbative part which we label ν_n, where n is the power of the moment. These ν_n come from forward proton matrix elements of local operators, and hence are amenable to lattice calculations

$$\left\langle N(p,s') \left| \mathcal{O}_q^{\{\mu_1 \ldots \mu_n\}} \right| N(p,s) \right\rangle = 2\bar{u}(p,s') \nu_n^{(q)} p^{\{\mu_1 \ldots \mu_n\}} u(p,s), \tag{3.109}$$

where $\{\ldots\}$ indicates symmetrisation of indices and the subtraction of traces.

Expressions similar to Eq. (3.108) exist for moments of other structure functions:

- unpolarised: $F_1/F_2/F_3 \leftrightarrow \nu_n$,
- polarised: $g_1 \leftrightarrow a_n$, $g_2 \leftrightarrow a_n - d_n$,
- and transversity: $h_1 \leftrightarrow h_n$.

As our first example, we consider an operator $\mathcal{O}$ which contains a gamma matrix, similar to the electromagnetic current, and one or more covariant derivatives, where the number of derivatives depends on moment we are looking at

$$\mathcal{O}_q^{\{\mu_1 \ldots \mu_n\}} = (i)^{n-1} \bar{q} \gamma^{\mu_1} \overleftrightarrow{D}^{\mu_2} \ldots \overleftrightarrow{D}^{\mu_n} q, \tag{3.110}$$

$$\overleftrightarrow{D} = \frac{1}{2}\left(\overrightarrow{D} - \overleftarrow{D}\right). \tag{3.111}$$

On the lattice the covariant derivatives take their usual definitions by a finite difference

$$(\overrightarrow{D}_\mu \psi)(x) = \frac{1}{2}\left[U_\mu(x)\psi(x + a\hat{\mu}) - U_\mu^\dagger(x - a\hat{\mu})\psi(x - a\hat{\mu})\right], \tag{3.112}$$

$$(\overline{\psi}\, \overleftarrow{D}_\mu)(x) = \frac{1}{2}\left[\overline{\psi}(x + a\hat{\mu})U_\mu^\dagger(x) - \overline{\psi}(x - a\hat{\mu})U_\mu(x - a\hat{\mu})\right]. \tag{3.113}$$

The terms $\mathcal{O}(1/Q^2)$ in Eq. (3.108) are higher-twist contributions, which are suppressed at large Q^2. So our operators $\mathcal{O}$ here are all of twist two and provide the dominant contribution in the deep-inelastic (large-Q^2) limit.

Similarly, for the moments of polarised structure functions we consider a polarised nucleon state and the matrix element is now dependent on the orientation of the nucleon spin, s^μ,

$$\left\langle N(p,s') \left| \mathcal{O}_q^{5;\{\mu_1 \ldots \mu_n\}} \right| N(p,s) \right\rangle = \bar{u}(p,s') \frac{a_{n-1}^{(q)}}{n+1} s^{\{\mu_1} p^{\mu_2} \ldots p^{\mu_n\}} u(p,s). \tag{3.114}$$

Here the operator contains a γ_5, so this is the axial version of Eq. (3.110)

$$\mathcal{O}_q^{5;\{\mu_1\ldots\mu_n\}} = (i)^{n-1}\bar{q}\gamma^{\mu_1}\gamma^5\overleftrightarrow{D}^{\mu_2}\ldots\overleftrightarrow{D}^{\mu_n}q. \tag{3.115}$$

3.3.3.1 Moments of PDFs

The interpretation of v_n in terms of moments of PDFs $q(x)$ is

$$v_n^{(q)} = \int_0^1 dx\, x^{n-1}\left(q(x) + (-1)^n\bar{q}(x)\right) = \langle x^{n-1}\rangle_q\,, \tag{3.116}$$

where $q(x)$ ($\bar{q}(x)$) is the probability to find a quark (antiquark) with momentum fraction x. Similarly, in the polarised case we have a_n which are simply the moments of polarised PDFs:

$$a_n^{(q)} = 2\int_0^1 dx\, x^n\left(\Delta q(x) + (-1)^n\Delta\bar{q}(x)\right) = 2\langle x^n\rangle_{\Delta q}\,. \tag{3.117}$$

$\Delta q(x)$ here are written as

$$\Delta q(x) = q_+(x) - q_-(x), \tag{3.118}$$

where $q_+(x)$ ($q_-(x)$) is the "probability" of finding a quark with momentum fraction x and the direction of the helicity equal (opposite) to that of the proton. In particular,

$$\frac{1}{2}a_0^{(q)} = \langle 1\rangle_{\Delta q} = \Delta q \tag{3.119}$$

is the fraction of the nucleon spin carried by quarks of flavour q. Also, the axial charge g_A is just

$$g_A = \Delta u - \Delta d. \tag{3.120}$$

3.3.3.2 Operators

As we have seen, on the lattice we need to consider twist-2 operators. We start their definitions by first noting that by changing to Euclidean space from Minkowski space we replace the Lorentz group by the orthogonal group $\mathcal{O}(4)$. We also work in discrete space-time which reduces this to the hypercubic group $H(4) \subset \mathcal{O}(4)$, and since $H(4)$ is finite, mixings are possible [150]. In order to reduce operator mixing, it is useful to use certain operator combinations which reside in certain irreducible representations of $H(4)$. For example, if we look at v_2 there are two

different irreducible representations we can form that have different combinations of indices:

$$\mathcal{O}_{v_{2a}} = \mathcal{O}^{\{14\}}, \tag{3.121}$$

$$\mathcal{O}_{v_{2b}} = \mathcal{O}^{\{44\}} - \frac{1}{3}\left(\mathcal{O}^{\{11\}} + \mathcal{O}^{\{22\}} + \mathcal{O}^{\{33\}}\right); \tag{3.122}$$

the first index here is the gamma matrix, and the second index is the derivative. Since v_{2a} and v_{2b} are different representations of the same continuum operator, they should agree in the continuum limit. Similarly,

$$\mathcal{O}_{v_3} = \mathcal{O}^{\{114\}} - \frac{1}{2}\left(\mathcal{O}^{\{224\}} + \mathcal{O}^{\{334\}}\right), \tag{3.123}$$

$$\mathcal{O}_{v_4} = \mathcal{O}^{\{1144\}} + \mathcal{O}^{\{2233\}} - \mathcal{O}^{\{1133\}} - \mathcal{O}^{\{2244\}}, \tag{3.124}$$

provide access to higher moments. For more details on operator construction, see [150].

3.3.3.3 Extracting Moments

Now, we want to extract these moments from calculations of lattice three-point functions (Eq. (3.57)) using the methods outlined in Sect. 3.3.2. Let us take the v_{2a} operator as an example. In Minkowski space this operator takes the indices $\{01\}$

$$\mathcal{O}^M_{v_{2a}} = \mathcal{O}^M_{\{01\}} = \frac{1}{2}\bar{q}\left(\gamma_0^M \overleftrightarrow{D}_1 + \gamma_1^M \overleftrightarrow{D}_0\right) q, \tag{3.125}$$

and the matrix element from Eq. (3.82) can be written then as

$$\frac{i}{4}\left\langle N(p,s') \left| \bar{q}\left(\gamma_0^M \overleftrightarrow{D}_1 + \gamma_1^M \overleftrightarrow{D}_0\right) q \right| N(p,s) \right\rangle = \langle x \rangle^{(q)} \frac{1}{2}\bar{u}(p,s')\left(\gamma_0^M p_1 + \gamma_1^M p_0\right) u(p,s),$$

where we have used the more common notation for $v_2^{(q)} = \langle x \rangle^{(q)}$, denoting the fraction of the nucleon's momentum carried by the quarks with flavour q. After Euclideanisation of this operator,

$$\gamma_0^M = \gamma_4^E, \quad \gamma_i^M = -i\gamma_i^E, \quad p_4^E = ip_0^M \equiv iE(\boldsymbol{p}), \quad p_i^E = -p_i^M, \tag{3.126}$$

$$D_4 = -iD^{(M)_0}, \quad D_i = -D^{(M)_i}, \tag{3.127}$$

we can rewrite it as

$$\frac{i}{4}\left\langle N(p,s')\left|\bar{q}\left(\gamma_0^E \overleftrightarrow{D}_1 + \gamma_1^E \overleftrightarrow{D}_4\right)q\right|N(p,s)\right\rangle$$
$$= \langle x\rangle^{(q)} \frac{1}{2}\bar{u}(p,s')\left(-\gamma_4^E p_1 - \gamma_1^E E_N(\boldsymbol{p})\right)u(p,s)\,. \tag{3.128}$$

Now if we use the standard spin-projector for an unpolarised nucleon, $\Gamma_{\text{unpol}} = (1+\gamma_4)/2$, and

$$\mathcal{J} = \frac{1}{2}\left(-\gamma_4 p_1 - i\gamma_1 E_N(\boldsymbol{p})\right)\,\langle x\rangle^{(q)}\,, \tag{3.129}$$

in Eq. (3.81), we find that the ratio of three- and two-point functions becomes

$$R(t,\tau;\boldsymbol{p},\boldsymbol{p};\mathcal{O}_{v_{2a}},\Gamma_{\text{unpol}}) = \frac{G_{\Gamma_{\text{unpol}}}(t,\tau;\boldsymbol{p},\boldsymbol{p};\mathcal{O}_{v_{2a}})}{G_2(t,\boldsymbol{p})} = ip_1\langle x\rangle^{(q)}\,. \tag{3.130}$$

Following a similar process for v_{2b} leads to

$$R(t,\tau;\boldsymbol{p},\boldsymbol{p};\mathcal{O}_{v_{2b}}) = -\frac{E_{\boldsymbol{p}}^2 + \frac{1}{3}\boldsymbol{p}^2}{E_{\boldsymbol{p}}}\,\langle x\rangle^{(q)}\,. \tag{3.131}$$

So we can see that in order to determine $\langle x\rangle$ using the v_{2a} operator we have to work with nonzero momentum, while in case of v_{2b} we can work with zero momentum.

In Fig. 3.13 we present an example of lattice results for these ratios from the QCDSF collaboration [151]. Here we see excellent agreement for the two different representations v_{2a} and v_{2b} of the same continuum operator (here we are considering the up-quark contribution), even though we look at finite lattice spacing, at different choices of proton momentum.

3.3.3.4 Operator Renormalisation

Let us talk now briefly about operator renormalisation, which deserves its own set of lectures (see, for example, [152]); we will consider here just the basic ideas of renormalisation. The lattice itself is a regularisation scheme, and the matrix elements that we measure using lattice operators will be in the lattice scheme; they are so-called bare operators $\mathcal{O}_{\text{bare}}$. In order to compare a lattice calculation of an observable to that in the continuum, i.e. from experiment or phenomenology, we need to switch to a continuum regularisation scheme, e.g. $\overline{\text{MS}}$. This is done by applying some renormalisation constant

$$\mathcal{O}^{\mathcal{S}}(M) = Z_{\mathcal{O}}^{\mathcal{S}}(M)\mathcal{O}_{\text{bare}} \tag{3.132}$$

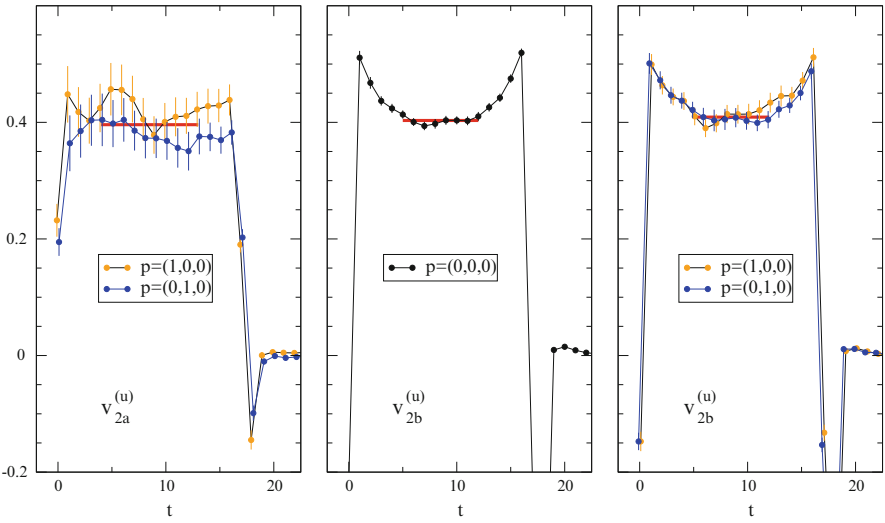

Fig. 3.13 Comparison of the ratios for v_{2a} in Eq. (3.130) and v_{2b} in Eq. (3.131) for a u-quark in the proton for different choices of momentum. Here the proton source and sink are placed at $t = 0$ and $t = 17$, respectively

(renormalise bare lattice operators in scheme $\mathcal{S}$ at scale M). We have mentioned mixing earlier, so if we have more operators with the same quantum numbers, but same or lower dimension, then we need to include mixings between these operators, i.e. we should actually include the sum of all of the contributions from the different lattice operators to get the result for the continuum operator:

$$\mathcal{O}_i^{\mathcal{S}}(M) = \sum_j Z^{\mathcal{S}}_{\mathcal{O}_i\mathcal{O}_j}(M,a)\mathcal{O}_j(a). \tag{3.133}$$

This procedure could in principle be done with lattice perturbation theory [12], however this is well known to be poorly convergent. We are then forced to revert to a nonperturbative method. The two commonly used methods are the Schrödinger functional [153] and the Rome-Southampton method [154].

For recent work computing these renormalisation constants for many lattice operators, see e.g. [155], and for a recent review of nonperturbative renormalisation, see [156].

3.3.4 Generalised Parton Distributions

We have seen in the previous section how parton distribution functions provide a description of the longitudinal momentum distributions of quarks and gluons in the nucleon. Although less well-understood, there is increasing interest in gaining

information on the transverse structure and angular-momentum distribution of partons within the nucleon. Generalised parton distributions (GPDs) [157–159] have opened new ways of studying the complex interplay of longitudinal momentum and transverse coordinate space [160, 161], as well as spin and orbital-angular-momentum degrees of freedom in the nucleon [162]. A full mapping of the parameter space spanned by GPDs is an extremely extensive task, which most probably needs support from nonperturbative techniques like lattice simulations. Given this interest, there has been a large amount of activity within the lattice community in the area of GPDs, and so we will devote some time here to summarising some of the important aspects relevant for lattice simulations.

3.3.4.1 Definition

The generalised parton distributions of quarks are defined at leading twist through the off-forward matrix elements of the light-cone operators

$$\begin{aligned}
&\int \frac{d\lambda}{4\pi}\, e^{i\lambda x}\, \left\langle P' \left| \overline{\psi}\,(-n\lambda/2)\, \gamma^\mu \psi\,(n\lambda/2) \right| P \right\rangle = \\
&\qquad\qquad \overline{U}(P') \left(\gamma^\mu H(x,\xi,t) + \frac{i\sigma^{\mu\nu}\Delta_\nu}{2m} E(x,\xi,t) \right) U(P)\,, \\
&\int \frac{d\lambda}{4\pi}\, e^{i\lambda x}\, \left\langle P' \left| \overline{\psi}(-n\lambda/2)\gamma_5\gamma^\mu \psi(n\lambda/2) \right| P \right\rangle = \\
&\qquad\qquad \overline{U}(P') \left(\gamma_5\gamma^\mu \tilde{H}(x,\xi,t) + \frac{i\gamma_5\Delta^\mu}{2m} \tilde{E}(x,\xi,t) \right) U(P)\,, \quad (3.134)
\end{aligned}$$

for the helicity-independent and helicity-dependent distributions, respectively. We note that the expressions in Eq. (3.134) are only valid in the light-cone gauge where $n \cdot A = 0$, otherwise we would need to include a gauge link $\exp\left(-ig \int_{-\lambda/2}^{\lambda/2} d\alpha\, n \cdot A(\alpha n)\right)$ between the two quark fields to ensure gauge invariance.

Figure 3.14 shows the electron-proton scattering process relevant for GPDs. Here the proton stays intact as we had earlier for the determination of form factors, but the probe has enough resolution to identify a single quark, as was the case for deep-inelastic scattering. This process is known as deeply virtual Compton scattering (DVCS), and the final states to be detected here are the proton together with the scattered electron and a photon.

It is common to denote the momentum transfer (squared) in the context of GPDs by $\Delta = P' - P$ ($t = \Delta^2$). Using the light-cone vector n, we define the longitudinal momentum transfer by $\xi = -n \cdot \Delta/2$. The proper definition of the twist-2 tensor or quark helicity-flip GPDs H_T, E_T, $\tilde{H}_T$ and $\tilde{E}_T$ can be found in [163]. GPDs provide a solid framework in QCD to relate many different aspects of hadron physics, some of which we have already discussed in earlier sections

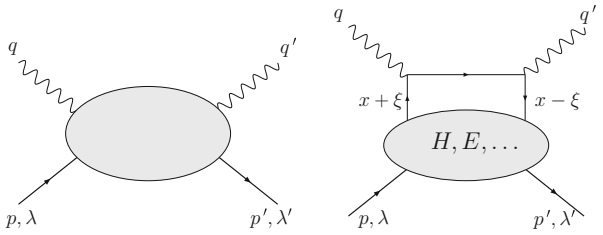

Fig. 3.14 Graphical representation of GPDs as part of a scattering amplitude

- The forward limit $\Delta \to 0$ of certain GPDs reproduces the well known parton distributions, that is $H(x, \xi = 0, t = 0) = q(x) = f_1(x)$, $\tilde{H}(x, 0, 0) = \Delta q(x) = g_1(x)$ and $H_T(x, 0, 0) = \delta q(x) = h_1(x)$.
- The integral over the longitudinal momentum fraction $\int dx$ of the GPDs gives the Dirac, Pauli, axial, pseudo-scalar, tensor etc. form factors, $\int dx\, H(x, \xi, t) = F_1(t)$, $\int dx\, E = F_2(t)$, $\int dx\, \tilde{H} = g_A(t)$, $\int dx\, \tilde{E} = g_P(t)$, $\int dx\, H_T = g_T(t)$ etc.
- The Fourier transforms $(2\pi)^{-2} \int d\Delta_\perp e^{-ib_\perp \cdot \Delta_\perp}$ of the GPDs H, $\tilde{H}$ and H_T at $\xi = 0$ are coordinate-space probability densities in the impact parameter $b_\perp$ [164].
- The forward limit of the x-moment of the GPD E, $\int dx\, x\, E(x, 0, 0) = B_{20}(0)$, allows for the determination of the quark orbital-angular-momentum contribution to the nucleon spin, $L^q = 1/2(\langle x \rangle + B_{20} - \Delta q)$, where $\langle x \rangle$ is the quark momentum fraction [162].

For more information on GPDs, see [165] for a review.

3.3.4.2 Matrix Elements and Moments of GPDs

For a lattice calculation of GPDs, we proceed in a similar way to our earlier discussion of structure functions by working in Mellin space to relate matrix elements of local operators to Mellin moments of the GPDs. But while for the moments of PDFs we considered forward ($t = 0$) matrix elements of the twist-2 operators defined in Eqs. (3.110) and (3.115), here we will use non-forward matrix elements of these same twist-2 operators. These matrix elements will specify the $(n-1)$th moments of the spin-averaged and spin-dependent generalised parton distributions, respectively. In particular, for the unpolarised GPDs, we have

$$\int_{-1}^{1} dx\, x^{n-1}\, H^q(x, \xi, t) = H_n^q(\xi, t)\,,$$
$$\int_{-1}^{1} dx\, x^{n-1}\, E^q(x, \xi, t) = E_n^q(\xi, t)\,, \tag{3.135}$$

where [162]

$$H_n^q(\xi,t) = \sum_{i=0}^{\lfloor\frac{n-1}{2}\rfloor} A_{n,2i}^q(t)(-2\xi)^{2i} + C_n^q(t)(-2\xi)^n|_{n\text{ even}}\,,$$

$$E_n^q(\xi,t) = \sum_{i=0}^{\lfloor\frac{n-1}{2}\rfloor} B_{n,2i}^q(t)(-2\xi)^{2i} - C_n^q(t)(-2\xi)^n|_{n\text{ even}}\,, \tag{3.136}$$

and the generalised form factors $A_{n,2i}^q(t)$, $B_{n,2i}^q(t)$ and $C_n^q(t)$ for the lowest three moments are extracted from the nucleon matrix elements [162]

$$\langle P'|\mathcal{O}_q^{\mu_1}|P\rangle = A_{10}^q(t)\,\bar{u}\,(P')\gamma^{\mu_1}u(P) + B_{10}^q(t)\,\bar{u}(P')\frac{i\sigma^{\mu_1\nu}\Delta_\nu}{2m}u(P)\,, \tag{3.137}$$

$$\langle P'|\mathcal{O}_q^{\{\mu_1\mu_2\}}|P\rangle = A_{20}^q(t)\,\bar{u}\,(P')\gamma^{\{\mu_1}u(P)\overline{P}^{\mu_2\}} \tag{3.138}$$

$$+\,B_{20}^q(t)\,\bar{u}(P')\frac{i\sigma^{\{\mu_1\nu}\Delta_\nu}{2m}u(P)\,\overline{P}^{\mu_2\}} + C_2^q(t)\,\frac{1}{m}\,\bar{u}(P')u(P)\,\Delta^{\{\mu_1}\Delta^{\mu_2\}}\,.$$

Note that the momentum transfer is given by $\Delta = P' - P$ with $t = \Delta^2$, while $\xi = -n\cdot\Delta/2$ denotes the longitudinal momentum transfer, and $\overline{P} = (P'+P)/2$ is the average nucleon momentum. We can construct an overdetermined set of equations to solve Eqs. (3.137), (3.138) for the generalised form factors, $A_{n,2i}^q(t)$, $B_{n,2i}^q(t)$ and $C_n^q(t)$. This technique is described in detail in [166].

For the lowest moment, A_{10} and B_{10} are just the Dirac and Pauli form factors F_1 and F_2, respectively:

$$\int_{-1}^{1} dx\,H^q(x,\xi,t) = A_{10}^q(t) = F_1(t)\,, \tag{3.139}$$

$$\int_{-1}^{1} dx\,E^q(x,\xi,t) = B_{10}^q(t) = F_2(t)\,, \tag{3.140}$$

while $\tilde{A}_{10}$ and $\tilde{B}_{10}$ are the usual axial-vector and pseudoscalar form factors, respectively

$$\int_{-1}^{1} dx\,\tilde{H}^q(x,\xi,t) = \tilde{A}_{10}^q(t) = g_A(t)\,, \tag{3.141}$$

$$\int_{-1}^{1} dx\,\tilde{E}^q(x,\xi,t) = \tilde{B}_{10}^q(t) = g_P(t)\,. \tag{3.142}$$

Similarly, the first moments of $H, E, \tilde{H}, \tilde{E}$ are explicitly

$$\int_{-1}^{1} dx\, x\, H^q(x,\xi,t) = A^q_{20}(t) + \xi^2 C^q_2(t)\,, \tag{3.143}$$

$$\int_{-1}^{1} dx\, x\, \tilde{H}^q(x,\xi,t) = \tilde{A}^q_{20}(t)\,, \tag{3.144}$$

$$\int_{-1}^{1} dx\, x\, E^q(x,\xi,t) = B^q_{20}(t) - \xi^2 C^q_2(t)\,, \tag{3.145}$$

$$\int_{-1}^{1} dx\, x\, \tilde{E}^q(x,\xi,t) = \tilde{B}^q_{20}(t)\,. \tag{3.146}$$

Note that there are no C form factors for the polarised moments.

We also observe that in the forward limit ($t = \xi = 0$) the moments of H_q reduce to the moments of the unpolarised parton distribution $A_{n0}(0) = \langle x^{n-1} \rangle$.

3.3.4.3 Transverse Densities

In the same way as we discussed in Sect. 3.2.1.3 for obtaining charge and magnetisation densities through two-dimensional Fourier transforms of electromagnetic form factors, Burkardt [161] has shown that generalised parton distributions gain a physical interpretation when Fourier transformed to impact parameter space at longitudinal momentum transfer $\xi = 0$. For example,

$$q(x, \boldsymbol{b}_\perp) = \int \frac{d^2\Delta_\perp}{(2\pi)^2}\, e^{-i\boldsymbol{b}_\perp\cdot\Delta_\perp} H(x,0,-\Delta^2_\perp)\,, \tag{3.147}$$

(and similarly for the polarised $\Delta q(x, \boldsymbol{b}_\perp)$) where $q(x, \boldsymbol{b}_\perp)$ is the probability density for a quark with longitudinal momentum fraction x and at transverse position (or impact parameter) $\boldsymbol{b}_\perp$.

Burkardt [161] also argued that $H(x,0,-\Delta^2_\perp)$ becomes $\Delta^2_\perp$-independent as $x \to 1$ since, physically, we expect the transverse size of the nucleon to decrease as x increases, i.e. $\lim_{x\to 1} q(x, \boldsymbol{b}_\perp) \propto \delta^2(\boldsymbol{b}_\perp)$. As a result, we expect the slopes of the moments of $H(x,0,-\Delta^2_\perp)$ in $\Delta^2_\perp$ to decrease as we proceed to higher moments. This is also true for the polarised moments of $\tilde{H}(x,0,-\Delta^2_\perp)$, so from Eq. (3.136) with $\xi = 0$ we expect that the slopes of the generalised form factors $A_{n0}(t)$ and $\tilde{A}_{n0}(t)$ should decrease with increasing n. This was clearly seen in several lattice simulations, e.g. [167, 168].

This idea was extended further to demonstrate how to use the first two moments of proton [169] and pion [170] GPDs to gain insights into the transverse spin distribution of hadrons. These results provided fascinating insights in to the complex interplay between hadron and quark spin orientation and the transverse distribution of quarks inside a hadron.

3.3.4.4 Nucleon Spin

As we have discussed earlier, it has been long known from DIS experiments that only about 30 % of the proton's spin is generated from the intrinsic spin of the quarks. This presents a puzzle as to how the remaining 70 % is generated through quark orbital angular momentum and by gluons.

Ji has provided a way forward by showing that the total quark and gluon angular momenta can be related to the second ($n = 2$) moments of the GPDs H and E [162]

$$J_{q,g} = \frac{1}{2}(A_{20}^{q,g}(0) + B_{20}^{q,g}) \,, \tag{3.148}$$

where $A_{20}(0)$ and $B_{20}(0)$ are the generalised form factors from Eq. (3.138) at zero momentum transfer ($t = 0$). We now have Ji's spin sum rule

$$\frac{1}{2} = \sum_q J_q + J_g \,. \tag{3.149}$$

The matrix elements in Eq. (3.138) can be computed on the lattice, and when combined with the further decomposition

$$J_q = \frac{1}{2}\Delta q + L_q \,, \tag{3.150}$$

together with a lattice determination of the quark spin fractions Δq from Sect. 3.3.2.2, we are able to not only provide a determination for the total amount of the proton's spin provided by the quarks, but also decompose this into quark spin and orbital angular momentum contributions.

As an example, we show in Fig. 3.15 results from QCDSF [171] (left) and LHPC [172] (right) for the total quark angular momentum contribution to the proton's

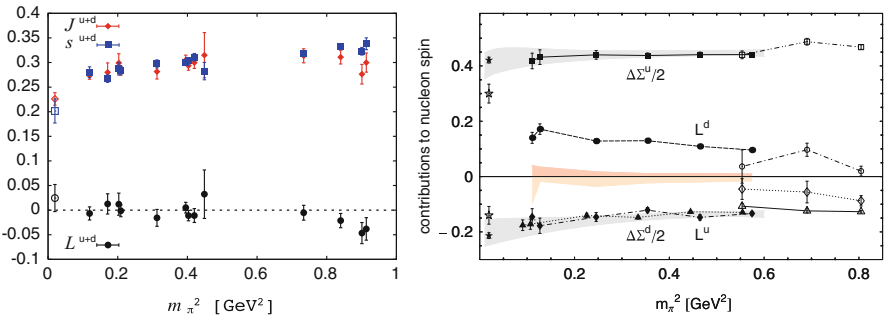

Fig. 3.15 Total angular momentum contribution of the quarks to the spin of the proton. Results are from QCDSF [171] (*left*) and LHPC [172] (*right*)

spin as a function of m_π^2 and its decomposition into helicity and orbital angular momentum contributions.

3.4 Summary

In these notes, we have studied various aspects of hadron structure, focusing on the nucleon, and how they can be studied on the lattice. We started with a discussion of elastic electron-proton scattering and how this leads to the idea of electromagnetic form factors and phenomenological implications for the distribution of charge (quarks) inside the nucleon.

By introducing the idea of deep-inelastic scattering (DIS), we motivated the idea of parton distribution functions (PDFs) and how this leads to description of distribution of momentum. These two ideas were combined into a general picture of the structure of the nucleon through the introduction of generalised parton distributions (GPDs). From these generalised functions, we saw how we can gain insights into transverse densities and decomposition of the spin of the nucleon into its quark and gluon constituents.

From the lattice side, we have learnt how we can determine the nonperturbative matrix elements relevant for these phenomenological quantities on the lattice. To do this, we introduced lattice three-point functions and showed how we can extract these matrix elements via ratios of three-point to two-point functions. We demonstrated the use of these lattice methods by providing some typical examples of recent lattice results of phenomenologically interesting quantities, such as the electromagnetic form factors F_1 and F_2, the average momentum fraction $\langle x \rangle$, the axial coupling constant g_A, and moments of generalised parton distributions.

Acknowledgements We would like to thank the organisers for putting together such a wonderful school. JMZ is supported by the Australian Research Council grant FT100100005.